Tryptophan-Free Human PNP Reveals Catalytic Site Interactions[†]

Mahmoud Ghanem,[‡] Suwipa Saen-oon,[§] Nickolay Zhadin,[‡] Corin Wing,[‡] Sean M. Cahill,[‡] Steven D. Schwartz,[§] Robert Callender,[‡] and Vern L. Schramm*[,‡]

Departments of Biochemistry and Physiology and Biophysics, Albert Einstein College of Medicine, Bronx, New York 10461

Received December 20, 2007; Revised Manuscript Received January 11, 2008

ABSTRACT: Human purine nucleoside phosphorylase (PNP) is a homotrimer, containing three nonconserved tryptophan residues at positions 16, 94, and 178, all remote from the catalytic site. The Trp residues were replaced with Tyr to produce Trp-free PNP (Leuko-PNP). Leuko-PNP showed near-normal kinetic properties. It was used (1) to determine the tautomeric form of guanine that produces strong fluorescence when bound to PNP, (2) for thermodynamic binding analysis of binary and ternary complexes with substrates, (3) in temperature-jump perturbation of complexes for evidence of multiple conformational complexes, and (4) to establish the ionization state of a catalytic site tyrosine involved in phosphate nucleophile activation. The ^{13}C NMR spectrum of guanine bound to Leuko-PNP, its fluorescent properties, and molecular orbital electronic transition analysis establish that its fluorescence originates from the lowest singlet excited state of the N1H, 6-keto, N7H guanine tautomer. Binding of guanine and phosphate to PNP and Leuko-PNP are random, with decreased affinity for formation of ternary complexes. Pre-steady-state kinetics and temperature-jump studies indicate that the ternary complex (enzyme–substrate−phosphate) forms in single binding steps without kinetically significant protein conformational changes as monitored by guanine fluorescence. Spectral changes of Leuko-PNP upon phosphate binding establish that the hydroxyl of Tyr88 is not ionized to the phenolate anion when phosphate is bound. A loop region (residues 243–266) near the purine base becomes highly ordered upon substrate/inhibitor binding. A single Trp residue was introduced into the catalytic loop of Leuko-PNP (Y249W-Leuko-PNP) to determine effects on catalysis and to introduce a fluorescence catalytic site probe. Although Y249W-Leuko-PNP is highly fluorescent and catalytically active, substrate binding did not perturb the fluorescence. Thermodynamic boxes, constructed to characterize the binding of phosphate, guanine, and hypoxanthine to native, Leuko-, and Y249W-Leuko-PNPs, establish that Leuko-PNP provides a versatile protein scaffold for introduction of specific Trp catalytic site probes.

Human purine nucleoside phosphorylase (PNP)[1] is a purine salvage enzyme that catalyzes the reversible phosphorolysis of 6-oxopurine nucleosides and deoxynucleosides to the corresponding purine bases and α-D-(deoxy)-ribose-1-phosphate (*1–6*). Transition-state analogue inhibitors of PNP provide potential therapies for T-cell cancers and autoimmune diseases (*7–9*). Crystal structures of PNP complexed with substrate analogues or transition-state inhibitors have defined the active site residues in contact with the purine nucleoside and the phosphate nucleophile (Figure 1) (*9–11*). The side chains of Glu201 and Asn243 form hydrogen bond contacts with N1H and N7H of the purine base, respectively (Figure 1) (*4, 10*).

PNP contains three nonconserved tryptophan residues at positions 16, 94, and 178, which are all remote from the catalytic site (Figure 1). A catalytic site loop (residues 243–266) is positioned near the purine base and the 5′-hydroxyl of bound nucleosides. It is highly ordered in the complex of PNP with Immucillin-H and phosphate and less ordered in unliganded PNP (*4, 12, 13*). A conformational change occurs in the loop upon guanine binding. Residues 241–260 act as a gate that opens during substrate binding (*10*). It has been hypothesized that the flexible active site loop reorganizes to allow different substrates/inhibitors to gain access to the active site of PNP (*4, 12, 14*). In agreement with that hypothesis, the superimposition of ligand-free PNP and PNP in complex with Immucillin-H and phosphate showed significant loop rearrangement (*4*). Thus, the active site loop of PNP is proposed to play a dynamic role in binding/catalysis. Similar changes have been reported in other nucleoside phosphorylases such as *Trypanosoma vivax* PNP (*15*). Therefore, probes of catalytic loop motion in PNP are of interest in catalysis.

Fluorescence is a sensitive tool to probe catalytic loop movement, and a catalytic site probe is provided by the intrinsic fluorescence of bound guanine, in contrast to free guanine or bound guanosine, which are not fluorescent. The chemical basis for this fluorescence is in debate (*16–26*). First, it was assumed that fluorescence of bound guanine was

[†] Supported by NIH research grants GM41916 and GM0680362.

* Corresponding author. E-mail: vern@aecom.yu.edu. Telephone: (718) 430-2813. Fax: 718-430-8565.

[‡] Department of Biochemistry, Albert Einstein College of Medicine.

[§] Department of Physiology and Biophysics, Albert Einstein College of Medicine.

[1] Abbreviations: PNP, native human purine nucleoside phosphorylase; Leuko-PNP, a chromophore-free mutant form of PNP with all three tryptophan residues (W16, W94, and W178) replaced with tyrosine residues; Y249W-Leuko-PNP, mutant form of Leuko-PNP with tyrosine 249 replaced by tryptophan.

10.1021/bi702491d CCC: $40.75
Published on Web 02/13/2008

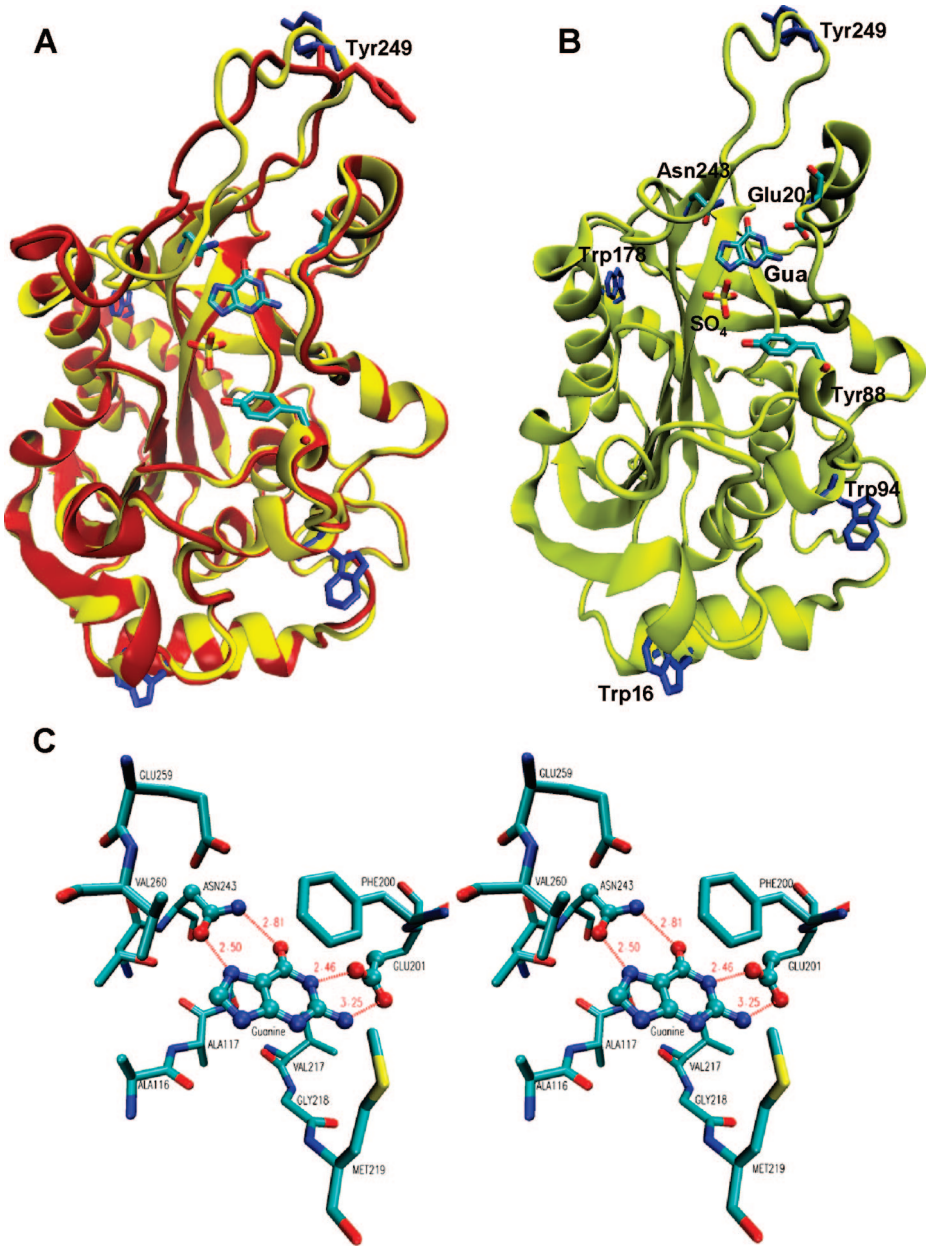

FIGURE 1: (A) Superimposition of the crystal structure of apo human PNP (red, PDB code 1M73) and human PNP bound to guanine, in the presence of sulfate (yellow, PDB code 1V2H). (B) Monomeric crystal structure of human PNP bound to guanine in the presence of sulfate (PDB code 1V2H). (C) Stereo figure of the model of guanine bound in the active site of PNP for the two-layer ONIOM calculations. Atoms shown in ball and stick style represent the *model-layer* treated with *high-level* calculations.

due to the preferential binding of anionic guanine, which is highly fluorescent, after ionization of the N1H of the base ($pK_a = 9.2$) (*16, 18–20*). Thereafter, structural, pH dependencies, steady-state, and pre-steady-state kinetics supported the idea that bound guanine exists as a neutral species (*17, 18, 21–24, 26*). Therefore, the nature of the fluorescent species of bound guanine has remained elusive. NMR, fluorescence properties, and computational chemistry reported here establish the electronic structure of bound guanine.

Replacement of the three nonconserved Trp residues with Tyr produced a chromophore-free PNP (Leuko-PNP) to probe the nature of bound fluorescent guanine and the protein conformational change upon the ligand binding by guanine fluorescence, T-jump, and ^{13}C NMR. A single tryptophan residue introduced into the catalytic loop (residues 243–266) of Leuko-PNP (Y249W-Leuko-PNP) was used to probe the loop environment upon hypoxanthine binding. With these probes, it is possible to monitor the pre-steady-state kinetics of guanine binding and guanosine phosphorolysis on PNP without interference from changes in protein tryptophan fluorescence.

MATERIALS AND METHODS

Site-Directed Mutagenesis. A QuikChange multisite-directed mutagenesis kit (Stratagene) was used to prepare the tryptophan-free PNP (Leuko-PNP), in which the three tryptophan residues (W16, 94, and 178) were replaced with tyrosines. The method was used according to the manufacturer's instructions, with the native PNP gene inserted into pCRT7/NT-TOPO (*27*) as a template and W16Y 5′-AAGATTATAAGAACACTGCAGAATATCTTCTGTCTCATACTAAGCACC-3′, W94Y 5′-TATGAAGGGTACCCACTCTACAAGGTGACATTCCCAGTG-3′, W178Y 5′-

Table 1: Comparison of Steady State Kinetic Constants and Inhibition Constants for Native, Leuko-, and Y249W-Leuko-PNPs with Inosine or Guanosine as Substrates and with Immucillin Inhibitors[a]

parameter	native PNP	Leuko-PNP	Y249W-Leuko-PNP
	Inosine as a Substrate		
k_{cat}, s^{-1}	44 ± 2	36 ± 1	30 ± 1
K_m, μM	71 ± 8	50 ± 3	35 ± 1
k_{cat}/K_m, M^{-1} s^{-1}	$(6.2 \pm 0.7) \times 10^5$	$(7.2 \pm 0.4) \times 10^5$	$(8.5 \pm 0.3) \times 10^5$
	Guanosine as a Substrate		
k_{cat}, s^{-1}	26 ± 1	23 ± 1	22 ± 1
K_m, μM	65 ± 12	55 ± 9	40 ± 4
k_{cat}/K_m, M^{-1} s^{-1}	$(4.0 \pm 0.7) \times 10^5$	$(4.2 \pm 0.5) \times 10^5$	$(5.5 \pm 0.6) \times 10^5$
	ImmH as an Inhibitor[b]		
K_i^*,[b] PM	88 ± 3	134 ± 12	163 ± 7
	DADMe-ImmH as an Inhibitor[b]		
K_i^*, PM	8.5 ± 0.3	12 ± 3	16 ± 3

[a] Enzymatic assays with either substrates or inhibitors were performed in 50 mM KH_2PO_4, pH 7.4, at 25 °C. [b] DADMe-ImmH, 4′-deaza-1′-aza-2′-deoxy-1′-(9-methylene)-Immucillin-H; ImmH, Immucillin-H; K_i^* slow-onset tight binding constant for inhibitors.

GAGGGCTCTCAGTACCTACAAACAAATGGGGGAGCAA-3′ oligonucleotides as primers (underlined letters indicate mismatches). The loop-tryptophan PNP mutant (Y249W-Leuko-PNP) was prepared using the Leuko-PNP gene inserted into pCRT7/NT-TOPO as a template and Y249Wf 5′-TAACAAGGTCATCATGGATTGGGAAAGC-CTGGAGAAGGC-3′, Y249Wr5′-GCCTTCTCCAGGCTTTC-CCAATCCATGATGACCTTGTTA-3′ oligonucleotides as forward (f) and reverse (r) primers, respectively (underlined letters indicate mismatches). The DNA sequence of the two mutants was confirmed, and the plasmid was transformed into *E. coli* strain BL21(DE3)pLysS competent cells (Invitrogen).

Expression and Purification of Leuko-PNP and Y249W-Leuko-PNP. Native PNP, Leuko-PNP, and Y249W-Leuko-PNP were expressed and purified to homogeneity as judged by SDS-PAGE using the same procedure used previously for the purification of the native PNP (*27*).

Preparation of Hypoxanthine-Free PNPs. Native PNP, Leuko-PNP, and Y249W-Leuko-PNP, as purified in 20 mM Tris-Cl, pH 7.4, contained tightly bound hypoxanthine in a stoichiometry of ~0.7–1 per monomeric enzyme concentrations, indicating that at least two out of the three active sites of the enzyme trimer are fully occupied with hypoxanthine. Incubation of the enzymes in 100 mM KH_2PO_4 in the presence of 10% charcoal (w/v) for 5 min followed by centrifugation and filtration of the enzyme resulted in the preparation of hypoxanthine-free PNPs.

Enzyme Assays. Activity assays for PNPs with inosine as a substrate were carried out as previously described by monitoring the conversion of hypoxanthine to uric acid (ϵ_{293} = 12.9 mM^{-1} cm^{-1}) (*28*) in a coupled assay containing 60 milliunits of xanthine oxidase and variable concentrations of inosine, in 50 mM KH_2PO_4, pH 7.4, at 25 °C (*29*). Activity assays for PNPs with guanosine monitored the formation of guanine (ϵ_{257} = −5.07 mM^{-1} cm^{-1}) in direct assays containing variable concentrations of guanosine, in 50 mM KH_2PO_4, pH 7.4, at 25 °C. The slow onset of inhibition was measured following the addition of enzyme to complete assay mixtures at 1 mM inosine and various inhibitor concentrations (*30, 31*). Inhibitor concentrations were determined spectrophotometrically using the published millimolar extinction coefficient of 9.54 at 261 nm at pH 7 for 9-deazainosine (ImmH based inhibitors) (*31–33*). Enzyme (0.2–0.5 nM final concentration) was added to assay mixtures followed by monitoring of product formation. Rates were monitored for 1–2 h to determine both the initial reaction rate and to determine if slow-onset inhibition occurred.

Fluorometric Titration of Enzymes. The fluorescence emission spectra (λ_{exc} = 295 nm, 2.5 nm slit width, and 10 mm path length) of the free or the ligand-bound PNP, Leuko-PNP, and Y249W-Leuko-PNP were acquired using a Fluro-Max-3 spectrofluorometer thermostatted at 25 °C. The dissociation constants for different ligands were obtained from the fluorometric titrations of the hypoxanthine-free PNPs (3 μM) with different ligands (phosphate, guanine for Leuko-PNP in the presence and the absence of 100 mM phosphate, and hypoxanthine for Y249W-Leuko-PNP in the presence and the absence of 100 mM phosphate) at pH 7.4. Typically, during titrations, the dilution does not exceed 10%, and all the fluorescence emissions spectra were corrected for dilution. Guanine and hypoxanthine stock solutions were prepared fresh prior to each titration, and their concentrations were determined spectrophotometrically using the published millimolar extinction coefficients of 10.7 mM^{-1} cm^{-1} at 246 nm and 10.7 mM^{-1} cm^{-1}at 250 nm at pH 7 for guanine and hypoxanthine, respectively (*34*).

Ultrafiltration Binding Study. Binding stoichiometries and dissociation constants of the three species of enzyme to either [8-^{14}C]guanine or [8-^{14}C]hypoxanthine were determined using a modification of the ultrafiltration method (*35–38*). The ultrafiltration apparatus was assembled with dialysis membrane (10 kDa molecular mass retention limit) and dried under vacuum. Typically, 200 μL aliquots containing 3 μM final enzyme concentration and variable concentrations (0.1–10 μM) of either [8-^{14}C]guanine or [8-^{14}C]hypoxanthine, in 100 mM KH_2PO_4, pH 7.4, were added to the upper wells of the ultrafiltration apparatus. The system was pressurized to ~20 psi with N_2 for ~60–90 min or until approximately half of the solution had passed into the lower well, and 30 μL aliquots were sampled from both upper and lower wells, added to 10 mL of scintillation fluid, and counted. Controls corrected for nonspecific binding to the enzyme and membrane.

Stopped-Flow Fluorescence Kinetics. The temperature dependence of guanine binding to Leuko-PNP and hypo-

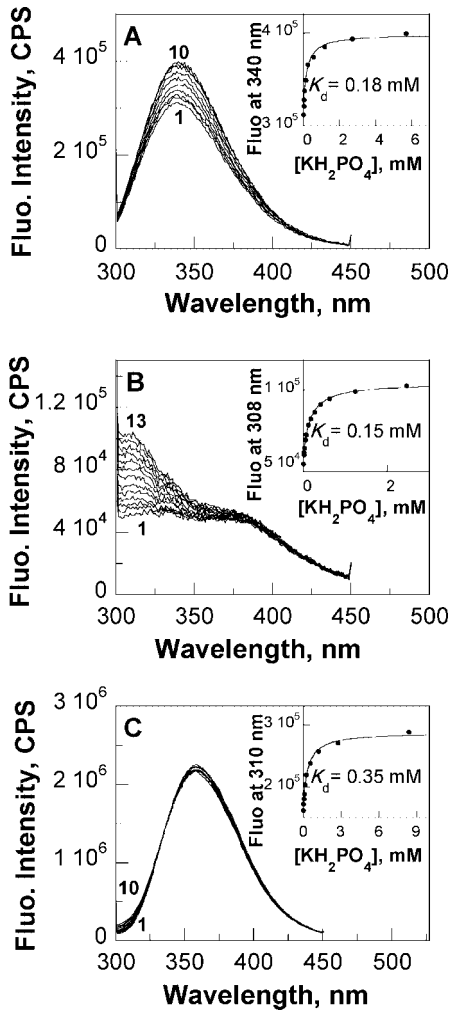

FIGURE 2: Binding of phosphate to PNPs. Fluorescence emission spectra (λ_{ex} = 295 nm) of native PNP (panel A), Leuko-PNP (panel B), and Y249W-Leuko-PNP (panel C) during the fluorometric titration of phosphate in a concentration range between 0 (curves 1, panels A, B, and C) and 5.7 mM (curve 10, panel A), 2.5 mM (curve 13, panel B), or 8.4 mM (curve 10, panel C). Insets: fluorescence emission intensity values (●) at 340 nm (panel A), 308 nm (panel B), and 310 nm (panel C) as a function of phosphate concentration for native PNP, Leuko-PNP, and Y249W-Leuko-PNP, respectively; the curves are fits of the data to eq 1. Fluorescence emission spectra were recorded at enzyme concentrations of ~3 μM in 20 mM Tris-Cl, pH 7.4, at 25 °C.

xanthine binding to Y249W-Leuko-PNP was determined using an KinTek SF-MiniMixer stopped flow attached to a FluoroMax-3 Spectrofluorometer equipped with a thermostatted water bath by following the fluorescence increase above 300 nm upon excitation at 295 nm (10 nm slit widths, 10 mm path length). The reactions involved mixing equal volumes of ~6 μM enzyme in 100 mM KH_2PO_4, pH 7.4, against saturated ligand solutions (36 μM for guanine and 186 μM for hypoxanthine) in 100 mM KH_2PO_4, pH 7.4, in the temperature range between 1 and 20 °C. Data points (20−100) were recorded over the course of each reaction (0.02–0.1 s), and at least 3 runs were averaged for each temperature. The rates of guanine and hypoxanthine binding to Leuko-PNP and Y249W-Leuko-PNP, respectively, at different temperatures were determined by fitting the kinetic data to a single exponential equation using the software provided by the manufacturer.

T-Jump Measurement of Leuko-PNP-Guanine Complex. The relaxation kinetics of Trp-free PNP bound to guanine in the presence of phosphate were determined by methods described previously (*39–42*). Temperature jumps were induced by a pulse of infrared light (1.56 μm wavelength, 90–120 mJ energy, 1.5–2.0 mm diameter spot on the sample, 0.5 mm path length), generated by stimulated Raman shifting the fundamental emission (1.064 μm) of a Powerlite 7010 Q-switched Nd:YAG laser (Continuum, Santa Clara, CA), operating at 2 Hz, in a 1 m long cell filled with deuterium gas at 650 psi. Water absorbs the laser energy, and the temperature of the exposed volume increases in approximately 6 ns. The size of the T-jump was calibrated using the change of water IR absorption with temperature. Typical T-jump values ranged from 6.5 to 8.5 °C. Diffusion of heat out of the interaction volume proceeds with a time constant of approximately 35 ms. Hence, the apparatus generated a T-jump within 6 ns that remained constant until approximately 10 ms.

The fluorescence intensity of the tryptophan fluorophore involved irradiation by emission lines near »290–300 nm from an Innova 200–25/5 argon ion laser (Coherent, Palo Alto, CA). To avoid photodamage, the excitation light was modulated using a shutter that allowed 12 ms exposure for every T-jump pulse. The power of the excitation beam was attenuated by neutral density filters to give a typical beam intensity of 15–20 mW. The incident excitation beam is focused onto a 0.3 mm diameter spot on the sample in the center of the beam path of the 1.56 μm pulse. Tryptophan fluorescence emission, detected at 50° to the excitation beam, was passed through a narrow band filter (340 ± 12 nm) and was monitored using a R4220P photomultiplier tube (Hamamatsu, Bridgewater, NJ). Data were digitized with a CS82G data acquisition board (Gage Applied Technologies, Montreal, Quebec, Canada) at 1 GS/s sampling rate. Overall temporal resolution of the system is about 20 ns. A background signal obtained without fluorescence excitation was measured separately and subtracted from the kinetic data. A program written in LabVIEW (National Instruments, Austin, TX) was used for instrument control and data collection. Data were normalized to the average fluorescence intensity taken before the T-jump.

Typically, T-jump relaxation profiles were obtained by subjecting the sample containing ~3 μM Leuko-PNP in 100 mM KH_2PO_4, pH 7.4, and variable concentration of guanine (0.45–72.5 μM) to a laser-induced temperature jump (from 20 to 27 °C) every 500 ms. The relaxation is monitored using fluorescence for the first 7 ms after the T-jump; once 300 ms has elapsed, the sample has relaxed to its original temperature, allowing the T-jump to be repeated. Each relaxation curve contains data from 3600 temperature jumps on the same sample. Curve fitting was done with OriginPro (OriginLab, Northampton, MA) software. The uncertainties in the reported values of relaxation rates were determined from the fitting parameters.

^{13}C NMR of the Leuko-PNP-Guanine Complex. [U-^{13}C, ^{15}N]Guanosine was purchased from Cambridge Isotope Laboratories. The ^{13}C NMR spectrum of the Leuko-PNP complex with labeled guanine was obtained by mixing ~700 μM of the enzyme with ~550 μM of labeled guanosine in 20 mM Tris-Cl and 10% D_2O, pH 7.4, and the mixture was subjected to arsenolysis using 50 mM Na_2HAsO_4 (Sigma).

Controls included the ^{13}C NMR spectra of labeled free guanosine at pH 7.4 and pH 12, the ^{13}C spectrum of labeled free guanine at pH 12 (prepared by arsenolysis and purified by reverse-phase HPLC), the ^{13}C spectrum of free Leuko-PNP, and the ^{13}C spectrum of the Leuko-PNP complexed with unlabeled guanine. All spectra were acquired using a Bruker 500 MHz spectrometer with 5 mm DUL $^{13}C(^{1}H)$ cryoprobe at 304 K. ^{13}C NMR spectra were collected with 15000 scans of 64 K points, a recycle delay of 2 s, and a carbon sweep width of 239 ppm with the carrier set to 100 ppm. Spectra were processed with an exponential window function of 5 Hz. The ^{13}C NMR spectra were assigned as described previously (*43, 44*).

Data Analysis. The dissociation constants and the stoichiometries of binding to PNPs were determined by fitting the fluorometric titrations data to either eq 1 or eq 2, where F_0, F_{EL}, and $F_{EL\infty}$ are the intrinsic fluorescence of the free enzyme, ligand-bound enzyme, and enzyme at saturating ligand, respectively, $[L]$ is the total ligand concentration, $[E_{act}]$ is the effective concentration of binding sites of the enzyme, f_E and f_{EL} are the fluorescence coefficients of free and ligand-bound enzyme, respectively, and K_d is the dissociation constant of the enzyme−ligand complex. The dissociation constants and stoichiometries of radiolabeled ligand binding to PNPs were determined by fitting the ultrafiltration equilibrium binding data to eq 3, where r is the moles of ligand bound per mole of enzyme, R is the moles of ligand bound per mole of enzyme at saturating ligand concentration, and A is the free ligand concentration. The temperature effects on the thermodynamics of guanine and hypoxanthine binding PNPs were determined by fitting the data to the Arrehenius equation (eq 4), where A is the preexponential factor, E_a is the energy of activation, R is the gas constant, with a value of 8.31 J mol^{-1} K^{-1}, and T is the temperature in Kelvin.

$$F_{EL} = \left(\frac{F_{EL\infty}[L]}{K_d + [L]}\right) + F_0 \quad (1)$$

$$F_{EL} = F_0 - (f_E - f_{EL})\left(\frac{[L]}{2} + \frac{[E_{act}]}{2} + \frac{K_d}{2} - \frac{\sqrt{([L] + [E_{act}] + K_d)^2 - 4[E_{act}][L]}}{2}\right) \quad (2)$$

$$1/r = (K_d/R)(1/A) + 1/R \quad (3)$$

$$\ln(k) = \ln A - [E_a/RT] \quad (4)$$

Excited-State Calculations. Time-dependent density functional theory (TD-DFT) was used to calculate the excited-state properties of guanine alone and in the Leuko-PNP complex (*45, 46*). The calculations used the triplet-ζ 6−311++G(d,p) basis set with the B3LYP exchange-correlation functional. Calculations were performed using Gaussian03 and the molecular orbitals rendered using the GaussView program (*47*).

The model of guanine bound in the active site of Leuko-PNP (Leuko-PNP-guanine) was generated from the X-ray structure of the PNP-guanine complex (PDB code: 1V2H (*10*)). The active site residues within 5 Å of guanine were included in the calculations. This model included guanine and Ala116, Ala117, Gly118, Phe200, Glu201, Val217, Gly218, Met219, Thr242, Asn243, Glu259, and Val260 (Figure 1C). Hydrogen atoms were added with GaussView,

Table 2: Comparison of the Physical and Spectral Properties of Native, Leuko-, and Y249W-Leuko-PNPs at pH 7.4

	native PNP	Leuko-PNP	Y249W-Leuko-PNP
Free Enzyme (E)[a]			
molecular mass/monomer, Da[b]	36101	36033	36056
tryptophan residues/monomer[b]	3	none	1
tyrosin residues/monomer[b]	10	13	12
predicted ϵ_{280} (mM^{-1} cm^{-1})[b]	28.83	19.62	23.63
crystallographic oligomeric state[c]	trimer	trimer	trimer
fluo. emission, $\lambda_{ex295\ nm}$ (λ_{max}, nm)[d]	∼340	na[e]	∼358
fluo. intensity, $\lambda_{ex295\ nm}$ (CPS)[d]	$\sim 3.5 \times 10^5$	$\sim 5 \times 10^4$	$\sim 1.5 \times 10^6$
Enzyme Phosphate Complex			
fluo. emission, $\lambda_{ex295\ nm}$ (λ_{max}, nm)[d]	∼340	∼308	∼358
Δ fluo. intensity ($E \cdot P_\infty - E$), $\lambda_{ex295\ nm}$ (CPS)	$\sim 1 \times 10^5$	$\sim 5 \times 10^4$	$\sim 0.1 \times 10^6$[f]
$K_{d\ (phosphate)}$ (mM)	0.18 ± 0.02	0.15 ± 0.01	0.35 ± 0.05
Enzyme Ligand Complex[g]			
fluo. emission, $\lambda_{ex295\ nm}$ (λ_{max}, nm)[d]	∼340	∼333	∼358
Δ fluo. intensity ($E \cdot L_\infty - E$), $\lambda_{ex295\ nm}$ (CPS)	$\sim 3.5 \times 10^5$	$\sim 3.5 \times 10^5$	$\sim 0.1 \times 10^6$
$K_{d\ (Gua/Hx)}$ (μM)	0.4 ± 0.1	0.26 ± 0.03	2.3 ± 0.7
stoichiometry ([L]:[E])	1.9 ± 0.2	1.5 ± 0.1	4.2 ± 1.1
Enzyme Phosphate Ligand Complex[g,h]			
fluo. emission, $\lambda_{ex295\ nm}$ (λ_{max}, nm)[d]	∼340	∼333	∼358
Δ fluo. intensity ($E \cdot P \cdot L_\infty - E \cdot P$), $\lambda_{ex295\ nm}$ (CPS)	$\sim 2 \times 10^5$	$\sim 1.3 \times 10^5$	$\sim 0.2 \times 10^6$
$K_{d\ (Gua/Hx)}$ (μM)	1.0 ± 0.2	0.68 ± 0.10	3.0 ± 0.8
stoichiometry ([L]:[E·P])	1.5 ± 0.5	1.50 ± 0.15	3.5 ± 1.0
Equilibrium Ultrafiltration Binding to Either [8-^{14}C]Guanine or [8-^{14}C]Hypoxanthine[i]			
$K_{d\ (Gua/Hx)}$ (μM)	0.53 ± 0.01	3.2 ± 0.3	1.3 ± 0.1
stoichiometry (*R*), mol/trimer	1.8 ± 0.1	3.3 ± 0.5	3.3 ± 0.8

[a] Enzyme in 20 mM Tris-Cl, pH 7.4. [b] Calculated from the amino acid sequence of the enzymes (*64*). [c] From ref (*10, 21*). [d] Fluorescence emission studies were carried out using ∼3μM of monomeric concentration of PNPs; CPS, count per second. [e] Not available. [f] The highest fluorescence intensity differences were observed at 310 nm. [g] Using guanine (Gua) for native and Leuko-PNPs and hypoxanthine (Hx) for Y249W-Leuko-PNP. [h] Enzymes in 100 mM KH_2PO_4, pH 7.4. [i] Using [8-^{14}C]guanine for native and Leuko-PNPs and [8-^{14}C]hypoxanthine for Y249W-Leuko-PNP in 100 mM KH_2PO_4, pH 7.4, at room temperature.

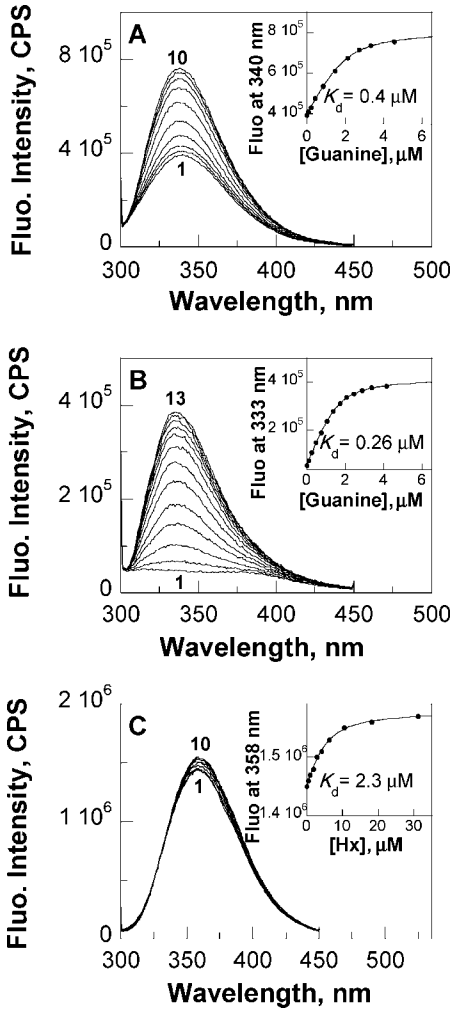

FIGURE 3: Ligand binding to PNPs in the absence of phosphate. Fluorescence emission spectra (λ_{ex} = 295 nm) of native PNP (panel A) and Leuko-PNP (panel B) during the fluorometric titration of guanine in a concentration range between 0 (panels A and B, curves 1) and 4.55 μM (panel A, curve 10) or 4.15 μM (panel B, curve 13), and Y249W-Leuko-PNP (panel C) during the fluorometric titration of hypoxanthine in a concentration range between 0 and 31.3 μM (panel C, curves 1 and 10, respectively). Insets: fluorescence emission intensity values (●) at 340 nm as a function of guanine (panel A), 333 nm as function of guanine (panel B), and 358 nm as a function of hypoxanthine (panel C) for native PNP, Leuko-PNP, and Y249W-Leuko-PNP, respectively; the curves are fits of the data to eq 2. Fluorescence emission spectra were recorded at enzyme concentrations of ~3 μM in 20 mM Tris-Cl, pH 7.4, at 25 °C.

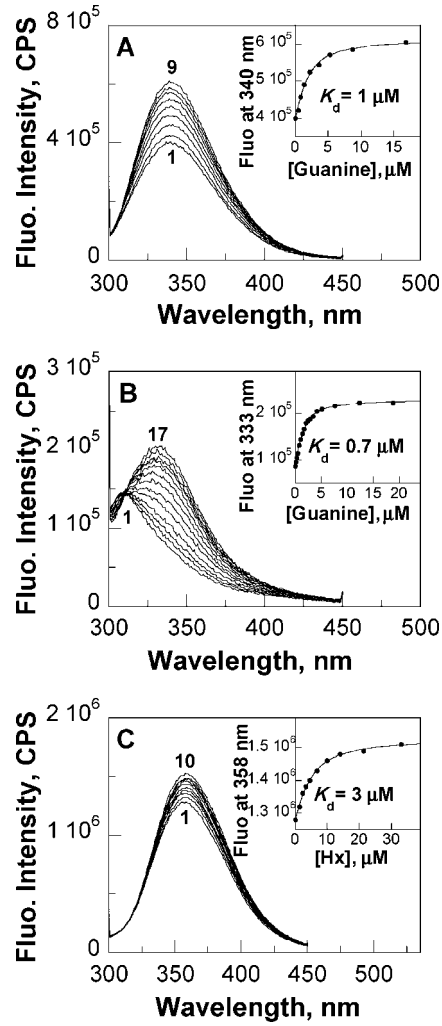

FIGURE 4: Ligand binding to PNPs in the presence of phosphate (PO_4). Fluorescence emission spectra (λ_{ex} = 295 nm) of native PNP-PO_4 and Leuko-PNP-PO_4 complexes during the fluorometric titration of guanine (panels A and B, respectively) in a concentration range between 0 and 17 μM (panel A, curves 1 and 9, respectively), and between 0 and 18.8 μM (panel B, curves 1 and 17, respectively), and Y249W-Leuko-PNP-PO_4 complex during the fluorometric titration of hypoxanthine in a concentration range between 0 and 33 μM (panel C, curves 1 and 10, respectively). Insets: fluorescence emission intensity values (●) at 340 nm as a function of guanine (panel A), 333 nm as a function of guanine (panel B), and 358 nm as a function of hypoxanthine (panel C) for native PNP-PO_4, Leuko-PNP-PO_4, and Y249W-Leuko-PNP-PO_4 complexes, respectively; the curves are fits of the data to eq 2. Fluorescence emission spectra were recorded at enzyme concentrations of ~3 μM in 100 mM KH_2PO_4, pH 7.4, at 25 °C.

assuming pH 7.4 where Glu201 and Glu259 have negatively charged carboxylates. In this calculation, only the N7H tautomeric form of guanine was considered since transition state analysis has established N7 protonation to N7H prior to reaching the transition state (*9*).

Three forms of N7H guanine were compared as (i) N1H, 6-keto, (ii) N1, 6-enol, and (iii) N1-anionic, 6-keto guanine for bound complex and for free guanine in gas phase. In gas phase calculations, free N7H guanine structures were optimized at the B3LYP/6−31G(d,p) level and followed by TD-DFT calculations at the B3LYP/6–311++G(d,p) level. Combined quantum mechanics and molecular mechanics (QM/MM) of the ONIOM method developed by Morokuma et al. (*48*) were used to study the Leuko-PNP-guanine complex. Two layers ONIOM (ONIOM2) calculations were applied by including guanine and the side chains of Asn243 and Glu201, which form strong H-bonds with the base into the *model-layer* treated with *high-level* (DFT) and the rest was treated with the semiempirical method (Figure 1C). The systems were optimized at the ONIOM2(B3LYP/6–31G(d,p):PM3) level and followed by excited-state TD-DFT calculations at the B3LYP/6–311++G(d,p) level for the *model-layer*.

RESULTS AND DISCUSSION

Expression and Purification of Leuko-PNP and Y249W-Leuko-PNP. Leuko-PNP and Y249W-Leuko-PNP were expressed and purified to homogeneity as judged by SDS-

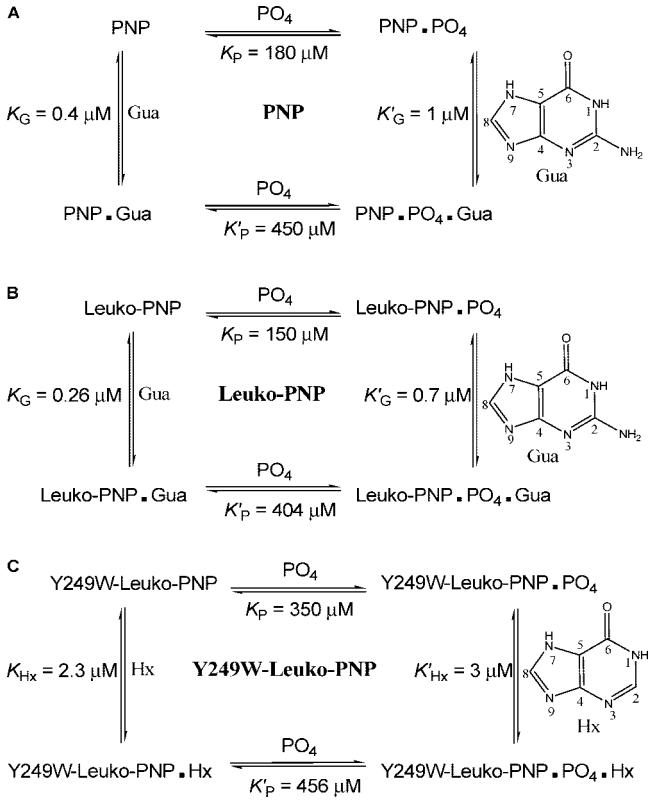

FIGURE 5: Comparison of the thermodynamic boxes for the binding of guanine to native PNP and Leuko-PNP (panels A and B, respectively) and the binding of hypoxanthine to Y249W-Leuko-PNP (panel C).

PAGE using the same procedure described previously for the purification of native PNP (*27*). Approximately 100 mg of pure enzyme was obtained from 1 L of Luria–Bertani culture medium. Native, Leuko-, and Y249W-Leuko-PNPs purified in 20 mM Tris-Cl, pH 7.4, contained tightly bound hypoxanthine in a stoichiometry of ~0.7–1 per catalytic site, as indicated by UV–visible spectroscopy or by HPLC after protein treatment with 10% (v:v) perchloric acid or 6 N HCl and removal of precipitated protein. Incubation of PNPs in 100 mM KH_2PO_4 in the presence of activated charcoal removes the hypoxanthine (less than 5% residual hypoxanthine per trimeric concentration of enzyme as indicated by reverse phase HPLC). This result is consistent with the previously described role of inorganic phosphate or arsenate in preventing the formation of tightly bound PNP-hypoxanthine complex (*35*). Native PNP expressed in *E. coli* is also isolated with tightly bound hypoxanthine, and this ligand can be removed from PNPs by the charcoal-phosphate treatment.

Steady State Kinetic and Slow Onset Inhibition Properties. The steady state kinetic parameters of the three species of PNP (PNP, Leuko-PNP, and Y249-Leuko-PNP) were determined with inosine and guanosine as substrates (Table 1). Leuko- and Y249W-Leuko-PNP are similar to PNP in their steady-state kinetic properties (Table 1). Although the catalytic efficiency (k_{cat}/K_m) of all three enzymes was similar, k_{cat} and K_m values of Leuko-PNP and Y249W-Leuko-PNP with either inosine or guanosine as substrate were slightly lower than those of native PNP (Table 1). Tighter binding of substrate/product correlating with slower turnover numbers (k_{cat}) is found when product release is a rate-limiting step in steady-state catalysis. Because the three PNPs are similar in

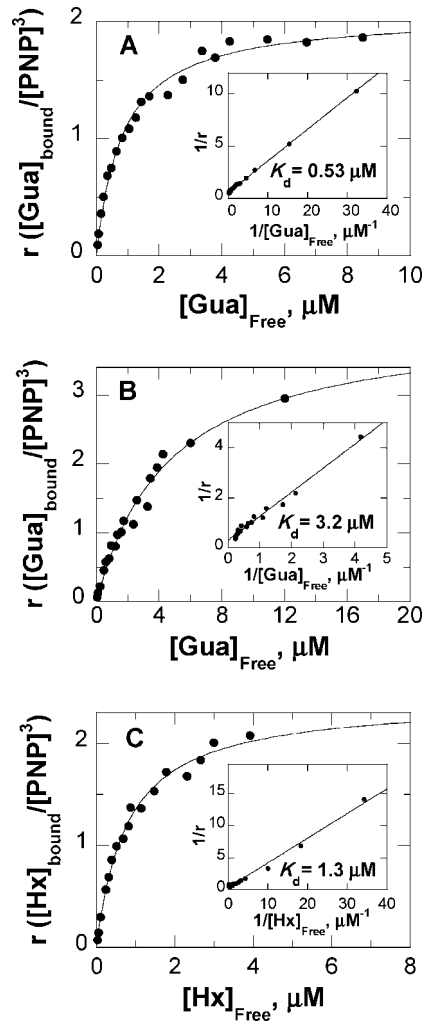

FIGURE 6: Equilibrium binding of [8-^{14}C]guanine or [8-^{14}C]hypoxanthine to PNPs in the presence of phosphate. Panels A and B, moles of [8-^{14}C]guanine per mole of enzyme (native PNP and Leuko-PNP, respectively) as a function of free [8-^{14}C]guanine. Panel C, moles of [8-^{14}C]hypoxanthine per mole of enzyme (Y249W-Leuko-PNP) as a function of free [8-^{14}C] hypoxanthine. Inset: double reciprocal plots of the equilibrium binding, curves are fits of the data to eq 3. All ultrafiltration binding experiments were at room temperature in the presence of 3 μM final enzyme concentration and variable concentrations (0.1 to 10 μM) of either [8-^{14}C]guanine or [8-^{14}C]hypoxanthine in 100 mM KH_2PO_4, pH 7.4.

catalytic efficiency (k_{cat}/K_m) and the rate-limiting step of some PNPs is known to be a release of purine, Y249-Leuko-PNP might be expected to exhibit the highest chemical rate (single turnover number), followed by Leuko-PNP and native PNP (*49*).

The differences in the dissociation constants for transition state analogues of PNP (Table 1) suggest differences in the transition-state structures as recently established in PNPs with mutations remote from the catalytic sites (*49–51*). Chromophore-free PNP (Leuko-PNP) and the loop-tryptophan-PNP (Y249W-Leuko-PNP) were employed to study ligand binding of PNP using spectrofluorometric techniques.

Spectrofluorometric Titrations of PNPs with Phosphate. Although the steady- and presteady-state spectrofluorometric properties of calf spleen and *Cellulomonas* PNPs have been reported (*18, 23–26*), these properties have not been reported for human PNP. The intrinsic fluorescence properties of the

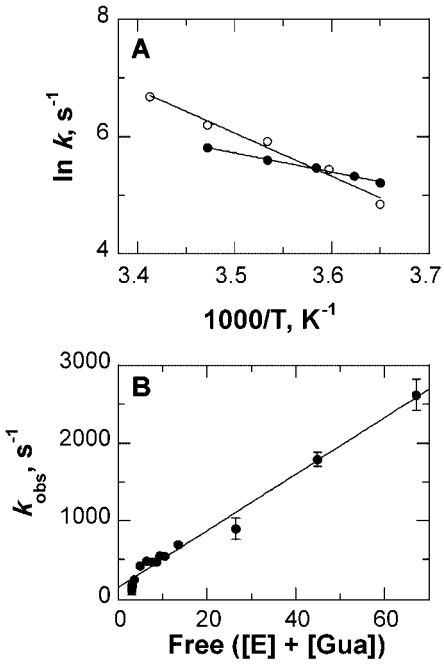

FIGURE 7: Association and dissociation rates for the binding of guanine (Gua) to Leuko-PNP and hypoxanthine (Hx) to Y249W-Leuko-PNP. Panel A, Arrhenius plot for the temperature dependence of the rates of guanine binding to Leuko-PNP (●) and the fluorescent changes in the active site loop of Y249W-Leuko-PNP due to hypoxanthine binding (○). The rates were recorded in the temperature range between 1 and 20 °C, in 100 mM KH_2PO_4, pH 7.4. Data were fit to eq 4 as indicated in Materials and Methods. Panel B, the concentration dependence of k_{obs} (●) for T-jump fluorescence relaxation profile of Leuko-PNP at different concentration of guanine (0.45–72.5 μM). All samples were prepared using 3 μM Leuko-PNP in 100 mM KH_2PO_4, pH 7.4 and excited at 300 nm and the emission were collected at 340 nm after temperature jump from ~20 to 27 °C.

PNPs were significantly different upon excitation at 295 nm (Figure 2 and Table 2). Native PNP (three Trp residues) showed emission maximum centered at 340 nm, while Leuko-PNP showed no emission maxima (Figure 2 and Table 2). The loop-tryptophan, Y249W-Leuko-PNP, showed an 18 nm shift of the emission maximum (λ_{max} centered at 358 nm) accompanied by 4-fold enhancement in the intrinsic fluorescence intensity relative to native PNP (Figure 2 and Table 2). This significant red-shift (18 nm) and enhanced intensity suggest a solvent exposed Trp residue in Y249W-Leuko-PNP with decreased quenching from neighboring residues relative to native PNP where the Trp residues are located in the hydrophobic core (*52, 53*).

Fluorometric titration of native PNP with inorganic phosphate gave a ~30% increase in the intrinsic fluorescence intensity at saturating ligand concentration without a shift of the emission maximum at 340 nm (Figure 2A and Table 2). A dissociation constant (K_d) of 0.18 ± 0.02 mM was determined by fitting the titration data to eq 1. This result is similar to the 20% enhancement of the intrinsic fluorescence intensity reported for the fluorometric titration of *Cellulomonas* PNP with inorganic phosphate (*25*). The 30% enhancement in the intrinsic fluorescence intensity of PNP is consistent with a small change in the environment of Trp249 and/or tyrosine residues (*52, 53*). Crystal structures of PNP complexed with guanine and sulfate (PDB code 1V2H) or complexed with Immucillin-H and phosphate (PDB code 1RR6) showed that Tyr88 is located within ~4 Å of bound phosphate or sulfate (Figure 1), suggesting ionization of Tyr88 (*10, 21, 54*). Fluorometric titration of Leuko-PNP with phosphate results in only small changes at 350 nm and the appearance of an emission maximum centered at 308 nm with 2-fold enhancement of fluorescence intensity compared to unliganded enzyme (Figure 2B and Table 2). A single dissociation constant (K_d) of 0.15 ± 0.01 mM was determined by fitting the titration data to eq 1 (Figure 2B and Table 2). Enhanced fluorescence intensity at 308 nm (characteristic fluorescence emission maximum for tyrosine) is inconsistent with ionization of Tyr88, suggesting polarity changes in the environment of Tyr88 and/or other Tyr residues (*54*). Titration of native PNP with phosphate indicated increased polarity in the Trp environments. Fluorometric titration of the loop-Trp-PNP (Y249W-Leuko-PNP) with inorganic phosphate caused no significant change in the fluorescence intensity at its λ_{max} at 358 nm (Figure 2C and Table 2). However, a small fluorescence intensity enhancement (6%) was observed at 310 nm, consistent with the change in the Tyr88 environment observed with Leuko-PNP (*54*). Similar to native PNP and Leuko-PNP, a dissociation constant (K_d) of 0.35 ± 0.05 mM was determined by fitting the titration data to eq 1 (Figure 2C and Table 2). In conclusion, there is no spectral evidence indicating ionization of a tyrosine hydroxyl upon phosphate binding in these PNPs.

Spectrofluorometric Titration of PNPs with Guanine. Fluorometric titration of native PNP with guanine in the absence or presence of phosphate (100 mM KH_2PO_4) showed 2-fold and 1.7-fold increase in fluorescence intensity, respectively, without a shift of the emission maxima (Figures 3A and 4A and Table 2). Titration data fitted to eq 2 gave K_d values of 0.4 ± 0.1 μM and 1.0 ± 0.2 μM for guanine in the absence and the presence of phosphate, respectively (Figures 3A and 4A and Table 2). Binding stoichiometries of 1.9 ± 0.2 and 1.5 ± 0.5 of guanine per trimer in the absence and the presence of phosphate, respectively (Table 2), suggest nonlinear fluorescence response to trimer saturation or two molecules of guanine bound per enzyme trimer. The structure of guanine bound to PNP to cause high fluorescence intensity is disputed (*16–26*). First, it was assumed that fluorescence intensity was due to N1-anionic guanine, which is highly fluorescent ($pK_a = 9.2$) (*16, 18–20*). Thereafter, structural, pH dependencies, steady-state, and pre-steady-state kinetics and binding studies supported the idea that guanine-bound PNP exists as the neutral species (*17, 18, 21–24, 26*).

Fluorometric titration of Leuko-PNP with guanine in the absence of phosphate showed a 7-fold increase of the fluorescence intensity with an emission maximum at 333 nm (Figure 3B and Table 2). This emission has no significant contribution from the protein and is consistent with N1H monoanionic guanine as previously reported (*16, 22*). A dissociation constant (K_d) value of 0.26 ± 0.03 μM and a stoichiometry of 1.5 ± 0.1 Gua/trimer resulted from fitting the titration data to eq 2 (Figure 3B and Table 2). Fluorometric titration of Leuko-PNP with guanine in the presence of phosphate (100 mM KH_2PO_4) showed a 2-fold increase in fluorescence intensity relative to the E-PO_4 complex and a bathochromic shift from 308 to 333 nm with a single isosbestic point at ~310 nm, consistent with a single process (Figure 4B and Table 2). A dissociation constant (K_d) value of 0.68 ± 0.10 μM and a stoichiometry of 1.50 ± 0.15 Gua/trimer were obtained from fitting the titration data to eq 2

Table 3: Comparison of the Association and Dissociation Rates for the Binding of Guanine (Gua) to Leuko-PNP and Hypoxanthine (Hx) to Y249W-Leuko-PNP in 100 mM KH_2PO_4, pH 7.4

	pre-steady-state fluorometry		T-jump	
enzyme	k_{on}, M^{-1} s^{-1}	k_{off}, s^{-1}	k_{on}, M^{-1} s^{-1}	k_{off}, s^{-1}
Leuko-PNP•PO_4•Gua	$(2.7 \pm 0.1) \times 10^{7a}$	86 ± 8^b	$(3.6 \pm 0.2) \times 10^{7c}$	142 ± 36^c
Y249W-Leuko-PNP•PO_4•Hx	$(1.3 \pm 0.1) \times 10^{7a}$	17 ± 1^b	nd[d]	nd

[a] Rates for 25 °C by extrapolating the stopped-flow fluorescence rates using the Arrhenius equation (eq 4). [b] Calculated [$K_d = k_{off}/k_{on}$] using the K_d values determined by ultrafiltration and k_{on} values determined by stopped-flow fluorometry. [c] Experimental rates obtained from the T-jump relaxation experiment. [d] Not determined.

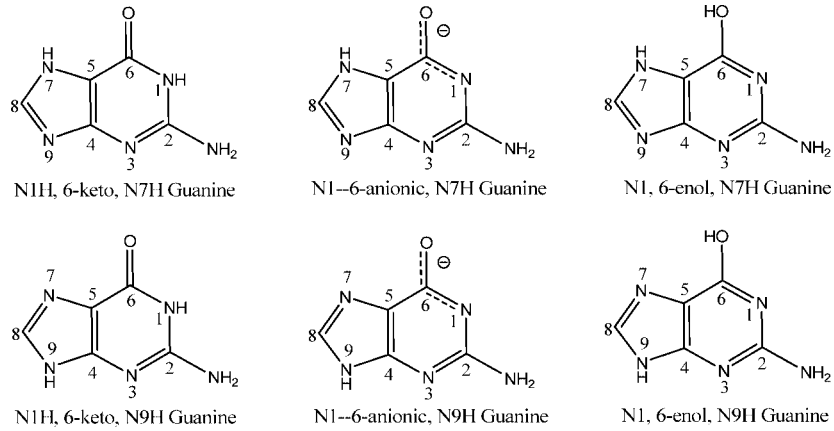

FIGURE 8: Molecular structures of different tautomers of guanine.

(Figure 4B and Table 2). Computational studies (see below) are used to identify the molecular structure corresponding to the spectral features of bound guanine.

Spectrofluorometric Titration with Hypoxanthine. Loop-Trp-PNP (Y249W-Leuko-PNP) was titrated with hypoxanthine to monitor catalytic site conformational changes in response to binding. Titrations of Y249W-Leuko-PNP with hypoxanthine in absence or the presence of phosphate (100 mM KH_2PO_4) showed a small increase in the intrinsic fluorescence intensity (~6–10%) without any shift of the emission maxima at 358 nm (Figures 3C and 4C and Table 2). The titration data were fitted to eq 2 to obtain K_d values of 2.3 ± 0.7 and 3.0 ± 0.8 μM for hypoxanthine in the absence and presence of phosphate, respectively (Figures 3C and 4C and Table 2). Binding stoichiometries of 4.2 ± 1.1 and 3.0 ± 1.3 per trimer were determined for hypoxanthine in the absence and the presence of phosphate, respectively (Table 2), consistent with binding of three molecules of hypoxanthine per enzyme trimer. The weak change in fluorescence for the single Trp PNP suggests that the reorganization of the catalytic site loop upon hypoxanthine binding leaves Trp249 in an environment unchanged from that of the empty catalytic site.

Thermodynamic boxes for the binding of guanine to native or Leuko-PNP and for hypoxanthine to Y249W-Leuko-PNP were solved from the dissociation constants determined from fluorometric titrations (Figure 5). All PNPs showed weaker binding to guanine or hypoxanthine in the presence of phosphate (Table 2). These results support a role for inorganic phosphate in facilitating purine base release following nucleoside phosphorolysis (*20, 35*). The binding affinity of ligands to the loop-Trp-PNP was 2- to 8-fold weaker than those for native PNP and Leuko-PNP and was most pronounced in binding of the purine base. In contrast, the K_m values for nucleosides (inosine or guanosine) decrease only slightly as a result of the Y249W-Leuko-PNP mutations (Table 1).

Equilibrium Ultrafiltration Binding. Fluorescence titrations depend on assumptions of linear response and complete saturation to permit accurate estimation of ligand stoichiometry. Binding parameters for guanine and hypoxanthine were also determined with [8-^{14}C]guanine and [8-^{14}C]hypoxanthine by equilibrium ultrafiltration (Figure 6 and Table 2). Dissociation constants for the binding of guanine to native PNP, Leuko-PNP, and of hypoxanthine to Y249W-Leuko-PNP were significantly larger than the values determined by fluorometric titrations. The binding stoichiometry of guanine to native PNP was 1.8 ± 0.1 mol/trimer, similar to the value from fluorescence titration. The results suggest negative cooperativity for filling the third catalytic site with guanine in native PNP. The binding stoichiometry for guanine binding to Leuko-PNP and for hypoxanthine binding to Y249W-Leuko-PNP was 3 mol/trimer (Table 2). These results agree with structural data in which each monomer of PNP contains a single active site saturated with substrate analogue (*21, 35, 55*). The dissociation constant of 1.3 ± 0.1 μM for hypoxanthine bound to the Y249W-Leuko-PNP-phosphate complex agrees well with the value of 1.6 μM determined in earlier studies (*35, 56*).

Association and Dissociation Binding Rates. The association and dissociation rates for guanine binding to Leuko-PNP-PO_4 and for hypoxanthine binding to Y249W-Leuko-PNP-PO_4 were determined by stopped-flow fluorometry and T-jump relaxation kinetics. The association rates from stopped-flow fluorometry for formation of PNP-(Gua/Hx)-PO_4 complexes for all PNPs increased monotonically with increasing temperature (Figure 7A). The rates of guanine association (k_{on}) with Leuko-PNP-PO_4 and hypoxanthine with Y249W-Leuko-PNP-PO_4 at 25 °C were determined to be $2.7 \pm 0.1 \times 10^7$ and $1.3 \pm 0.1 \times 10^7$ M^{-1} s^{-1},

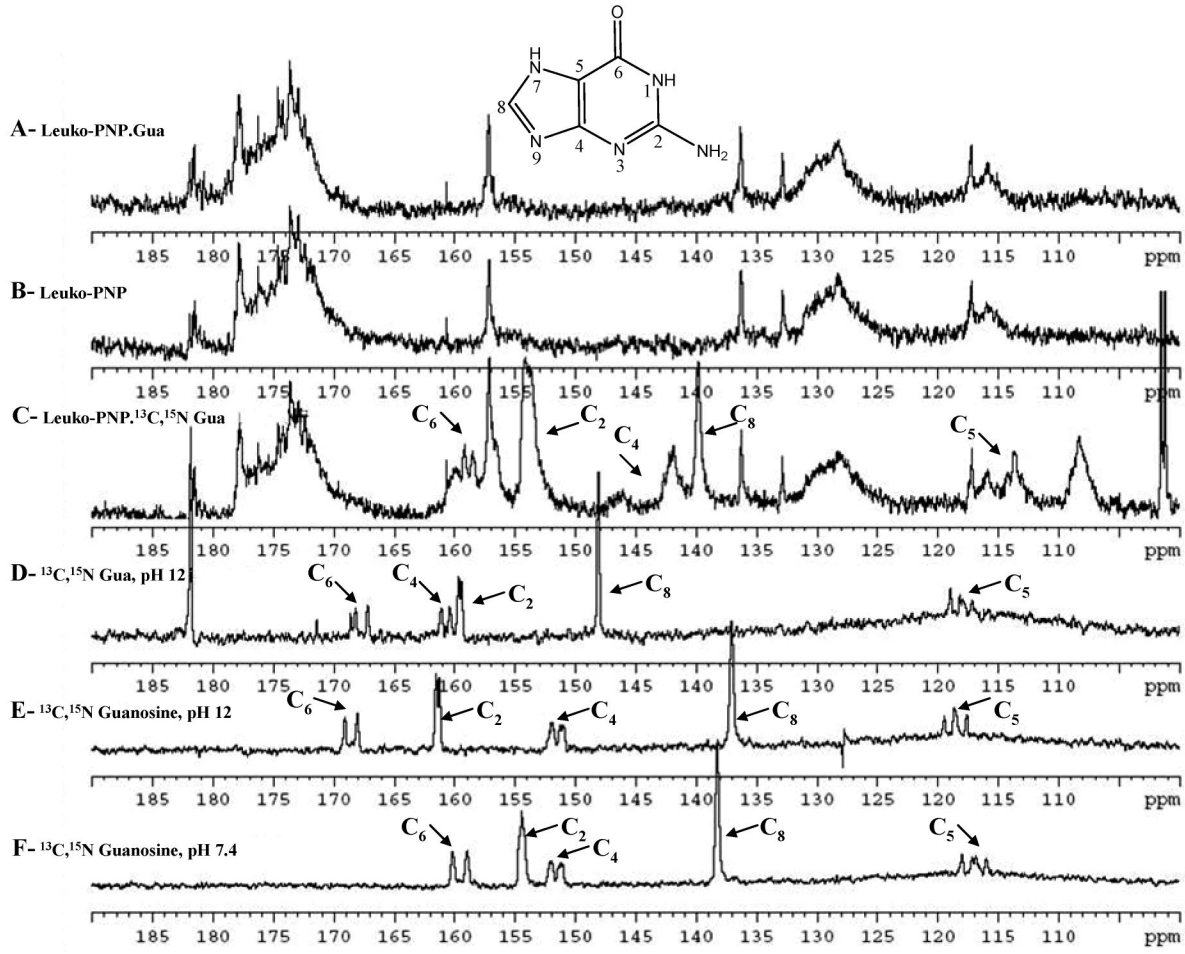

FIGURE 9: ^{13}C NMR spectra of (A) Leuko-PNP complexed with the unlabeled guanine (0.7 mM: 0.6 mM, pH 7.4), (B) free Leuko-PNP (0.7 mM, pH 7.4), (C) Leuko-PNP complexed with the ^{13}C,^{15}N-guanine (0.7 mM: 0.6 mM, pH 7.4), (D) free ^{13}C,^{15}N-guanine (0.6 mM, pH 12), (E) free ^{13}C,^{15}N-guanosine (0.6 mM, pH 12), and (F) free ^{13}C,^{15}N-guanosine (0.6 mM, pH 7.4). All ^{13}C spectra were acquired at room temperature in 90% H_2O and 10% D_2O with 20 mM Tris-Cl.

Table 4: TD-DFT Excitation Energies (λ) Calculated at the B3LYP/6–311G++(d,p)] Level

tautomeric form	orbitals[a]	oscillator strengths[b] (f)	λ_{calc}, nm [E, eV]	λ_{expt}, nm [E, eV][c]
		Free N7H Guanine		
				~340 [3.65]
N1H, 6-keto				
$S_0 \rightarrow S_1$	H → L	0.1122	269 [4.61]	
$S_0 \rightarrow S_2$	H → L + 1	0.0097	256 [4.84]	
N1, 6-enol				
$S_0 \rightarrow S_1$	H → L + 1	0.0005	297 [4.18]	
$S_0 \rightarrow S_2$	H → L	0.0696	289 [4.29]	
N1-anionic, 6-keto				
$S_0 \rightarrow S_1$	H → L	0.0029	392 [3.16]	
$S_0 \rightarrow S_2$	H → L + 1	0.0026	341 [3.63]	
		N7H Guanine Bound to Leuko-PNP		
				~333 [3.72]
N1H, 6-keto				
$S_0 \rightarrow S_1$	H → L	0.0008	342 [3.62]	
$S_0 \rightarrow S_2$	H → L + 1	0.0063	332 [3.73]	
N1, 6-enol				
$S_0 \rightarrow S_1$	H → L	0.0005	480 [2.58]	
$S_0 \rightarrow S_2$	H → L + 1	0.0001	458 [2.71]	
N1-anionic, 6-keto				
$S_0 \rightarrow S_1$	H → L	0.0002	900 [1.38]	
$S_0 \rightarrow S_2$	H-1 → L + 1	0.0001	660 [1.88]	

[a] H represents HOMO, L represents LUMO. [b] Oscillator strengths (f) are the dominant one-electron orbital contributions for the transitions. [c] [E, eV], calculated from the experimental fluorescence λ_{max} ($E = hc/\lambda$).

respectively, by extrapolating the experimental data using the Arrhenius equation (Figure 7A and Table 3). Dissociation rates (k_{off}) of 86 ± 8 and 17 ± 1 s^{-1} for guanine from Leuko-PNP-PO_4-guanine and for hypoxanthine from

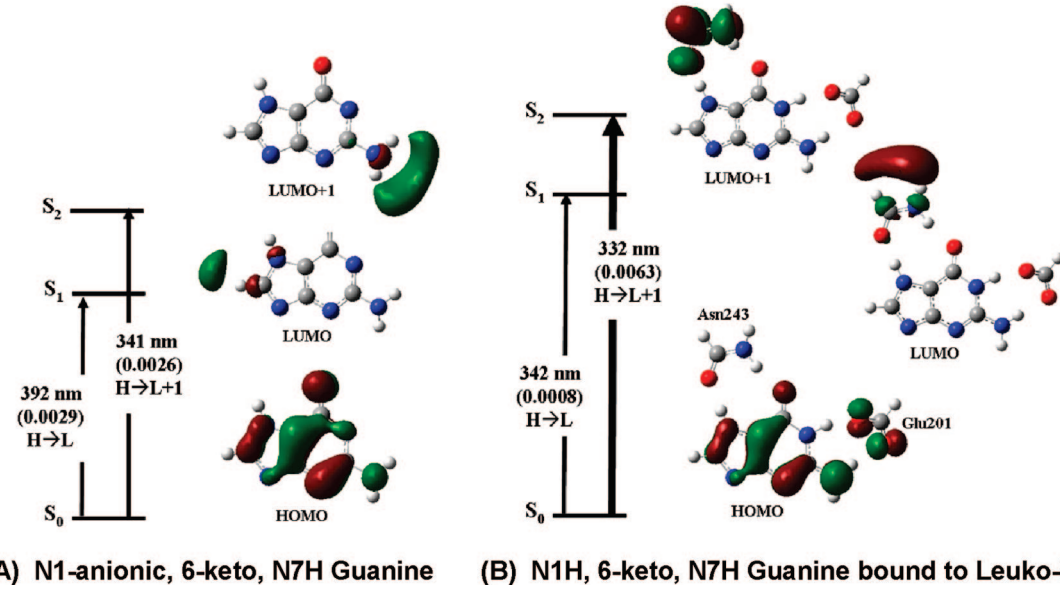

FIGURE 10: Jablonski diagram of singlet excited-state transitions of (A) N1-anionic, 6-keto, N7H guanine in gas phase and (B) N1H, 6-keto, N7H guanine bound to Leuko-PNP as determined by TD-DFT calculations at the B3LYP/6−311++G(d,p) level. Oscillator strengths are shown in parentheses as the dominant one-electron orbital contributions for the transitions. Molecular orbitals involved in the HOMO → LUMO and HOMO → LUMO + 1 electronic transition are shown. Different colors represent lobes of opposite sign. The widths of the lines denoting the excited-state transitions reflect the relative oscillator strengths of the transitions.

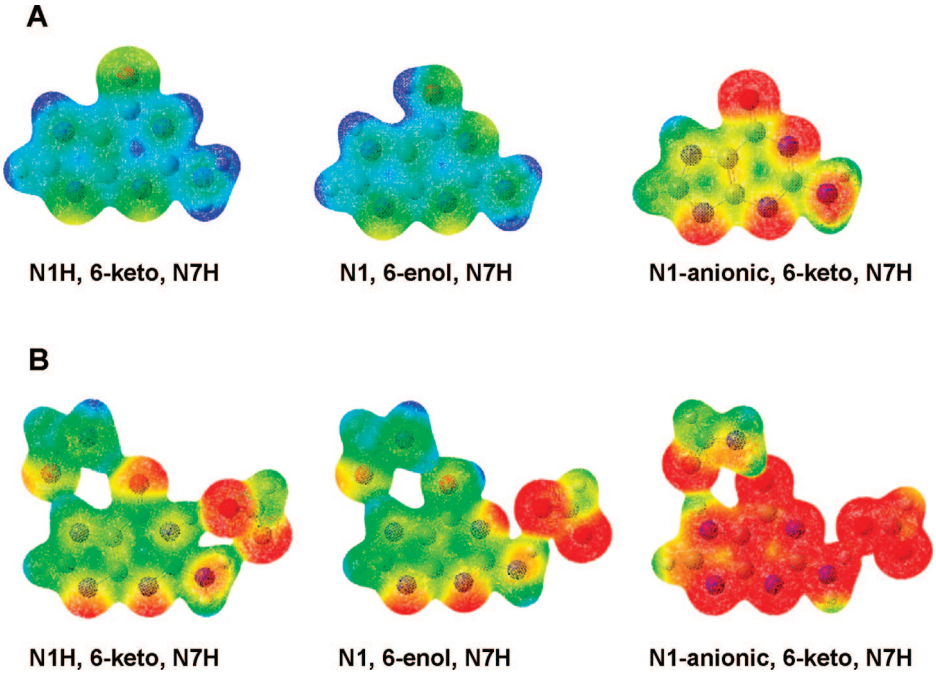

FIGURE 11: Electrostatic potential surface of three different tautomers of guanine in gas phase (panel A) and guanine bound to Leuko-PNP (panel B), calculated at the B3LYP/6–311++G(d,p) level of theory.

Y249W-Leuko-PNP-PO_4-hypoxanthine, respectively (25 °C), were calculated from the stopped-flow k_{on} and the ultrafiltration K_d values (Table 3).[2] In agreement with the k_{on} and k_{off} values determined for guanine using stopped-flow fluorometry, k_{on} and k_{off} values of $3.6 \pm 0.2 \times 10^7$ M^{-1} s^{-1} and 142 ± 36 s^{-1}, respectively, were determined for guanine association and dissociation from the Leuko-PNP-PO_4 complex using T-jump relaxation kinetics (Figure 7B and Table 3). The relatively tight binding and slow release of purine bases from PNP confirm that product release is the rate-limiting step for nucleoside phosphorolysis by PNP (*24, 58*). The small fluorescence signal for hypoxanthine binding to the loop-Trp-phosphate binary complex did not allow the experimental determination of the k_{on} value.

^{13}C NMR of the Leuko-PNP-Guanine Complex. The ^{13}C NMR spectra of guanine and the Leuko-PNP-guanine complex were used to explore the nature of bound guanine. The ab initio study of the excited states of free guanine in gas phase and aqueous media indicated that 6-keto, N7H guanine is the most stable form in the gas phase and 6-keto, N9H guanine is the most stable form in water (Figure 8) (*59*). However, the transition-state analysis PNP has established N7 protonation to N7H prior to reaching the transition state (*9*). The fluorescence peak of guanine in aqueous solution at 332 nm has been proposed to originate from the

lowest singlet excited state of the 6-keto, N7H guanine (Figure 8) (*59*). However, pH titrations of free guanine in 50 mM KH_2PO_4 showed that guanine is only fluorescent at high pH (above pH 8.5), with a fluorescent emission peak centered at ~340 nm (data not shown), consistent with ionization of the N1H of the base ($pK_a = 9.2$) (*16, 18–20*). The ^{13}C NMR spectra of guanine and guanosine were compared at high and physiological pH values. An 8 ppm, downfield shifts of C_2 and C_6 were observed in the ^{13}C NMR spectrum of guanosine at high pH relative to that at physiological pH (Figure 9). This shift is consistent with ionization of guanosine N1H (pK_a value of 9.2) to the anion. The ^{13}C NMR spectrum of free guanine at high pH showed a similar pattern for C_2 and C_6 chemical shifts (Figure 9). The ^{13}C NMR of Leuko-PNP-guanine was similar to ^{13}C-guanosine at neutral pH (Figure 9), consistent with neutral N1H guanine at the catalytic site. This spectrum also confirms that N1H is the H-bond donor to Glu201 (mammalian PNPs) or Glu204 (*Cellulomonas* PNP) (*17, 18, 21–24, 26*). Mutation of Glu201 to alanine or glutamine decreases both catalytic efficiency and the binding affinity of PNP for substrates and substrate analogues (*60*), consistent with the interaction at N1H being important in binding and catalysis.

Guanine Excited-State Calculations. The localized orbital picture was used to probe the guanine excited state. Electron transitions are described as linear combinations of one-electron promotions between occupied and unoccupied molecular orbitals (MOs) (*61*). The orbitals involved in these transitions were investigated for the N1-neutral (6-keto and 6-enol) guanine and the N1-anionic tautomeric forms of free N7H guanine and in complex with Leuko-PNP. In guanine, the promotion of an electron from the ground state to the lowest energy $\pi-\pi^*$ state mainly involves the highest occupied molecular orbital (HOMO) and the lowest unoccupied molecular orbital (LUMO) or LUMO + 1.

TD-DFT calculations of guanine in the gas phase indicate that N1-anionic, 6-keto, N7H guanine exhibits two transitions above 330 nm, while the N1H, 6-keto, N7H and N1, 6-enol, N7H forms fluoresce at 250 to 300 nm (Table 4 and Figures S2 and S3 of the Supporting Information). The $S_0 \rightarrow S_2$ (HOMO $\rightarrow$ LUMO + 1) transition of N1-anionic guanine has a transition wavelength at 341 nm, consistent with the experimental emission wavelength (λ_{max}) at 340 nm seen for guanine at high pH. Thus, both calculated and experimental fluorescent emission λ_{max} are consistent with N1-anionic, 6-keto, N7H guanine as the fluorescent tautomeric species of guanine in solution. However, the λ_{max} of 333 nm is established for guanine bound to Leuko-PNP at physiological pH. The ^{13}C NMR spectrum of guanine-Leuko-PNP establishes that fluorescent-bound guanine is not the N1-anion. TD-DFT calculations of N7H guanine bound to Leuko-PNP indicate that the $S_0 \rightarrow S_2$ (HOMO $\rightarrow$ LUMO + 1) transition of the N1H, 6-keto, N7H guanine has a transition wavelength at 332 nm, whereas the predicted transition wavelength of N1, 6-enol, N7H and anionic forms are above 450 nm. The electronic configurations of N1-anionic, 6-keto, N7H guanine and N1H, 6-keto, N7H guanine bound to Leuko-PNP are similar, with electron delocalization in the HOMO, excitation which dominates the ground-state contributions to the $S_0 \rightarrow S_1/S_2$ transitions (Figure 10). This induced electron delocalization in the HOMO of guanine bound to Leuko-PNP may be due to the strong hydrogen bond interaction of N1H with Glu201 ($r_{HO} = 1.64$ Å, $\angle_{NHO} = 162°$). The electronic changes through N1 are indicated by the electrostatic potential (ESP) surface and atomic ESP charges using the Merz–Singh–Kollman (MK) scheme (Figure 11 and Table S1 of the Supporting Information).

CONCLUSION

The results from fluorometric titrations, pre-steady-state kinetics, equilibrium ultrafiltration binding, and T-jump fluorometry support the formation of the catalytically relevant ternary complex (enzyme−ligand−phosphate) for PNP by random path single-step binding processes. In binding, at least two of the three catalytic sites of trimeric PNP act independently. In the presence of phosphate, the binding of guanine or hypoxanthine to PNP does not lead to protein conformational changes that generate unambiguous fluorescence signals from the reporter chromophores over the msec (stopped-flow) or the nsec to μsec (T-jump) time ranges. These results are consistent with a one-step binding process of noninteracting binding sites for the binding of hypoxanthine in the presence of phosphate. In the absence of phosphate, negative cooperativity between PNP binding sites has been observed for guanine or hypoxanthine and for the binding of transition-state analogue inhibitors (Immucillins) to mammalian PNPs in the presence of phosphate (*35, 62, 63*). The nature of fluorescent-bound guanine is established to be N1H, 6-keto, N7H guanine with altered electronic properties from catalytic site contacts. Leuko-PNP provides a novel, achromatic protein platform to investigate the interaction of chromophores with this important drug target.

SUPPORTING INFORMATION AVAILABLE

Arrhenius plot for the temperature dependence of the dissociation rates (k_{Off}) of guanine from Leuko-PNP (Figure S1), Jablonski diagram of singlet excited-state transitions of different N1-ionization of N7H guanine in gas phase as determined by TD-DFT calculation at the B3LYP/6–311++G(d,p) level (Figure S2), Jablonski diagram of singlet excited-state transitions of different N1-ionization of N7H guanine bound to Leuko-PNP as determined by TD-DFT calculations at the B3LYP/6–311++G(d,p) level (Figure S3), and the atomic charges using the Merz–Singh–Kollman (MK) scheme calculated at the B3LYP/6–311++G(d,p) level of theory (Table S1).This material is available free of charge via the Internet at http://pubs.acs.org.

REFERENCES

1. Giblett, E. R., Ammann, A. J., Wara, D. W., Sandman, R., and Diamond, L. K. (1975) Nucleoside-phosphorylase deficiency in a child with severely defective T-cell immunity and normal B-cell immunity. *Lancet 1*, 1010–1013.
2. Krenitsky, T. A., Tuttle, J. V., Koszalka, G. W., Chen, I. S., Beacham, L. M., III, Rideout, J. L., and Elion, G. B. (1976) Deoxycytidine kinase from calf thymus. Substrate and inhibitor specificity. *J. Biol. Chem. 251*, 4055–4061.
3. Mitchell, B. S., Mejias, E., Daddona, P. E., and Kelley, W. N. (1978) Purinogenic immunodeficiency diseases: selective toxicity of deoxyribonucleosides for T cells. *Proc. Natl. Acad. Sci. U.S.A. 75*, 5011–5014.
4. Núñez, S., Wing, C., Antoniou, D., Schramm, V. L., and Schwartz, S. D. (2006) Insight into catalytically relevant correlated motions in human purine nucleoside phosphorylase. *J. Phys. Chem. A 110*, 463–472.
5. Stoeckler, J. D., Cambor, C., and Parks, R. E., Jr. (1980) Human erythrocytic purine nucleoside phosphorylase: reaction with sugar-modified nucleoside substrates. *Biochemistry 19*, 102–107.

6. Ullman, B., Gudas, L. J., Clift, S. M., and Martin, D. W., Jr. (1979) Isolation and characterization of purine-nucleoside phosphorylase-deficient T-lymphoma cells and secondary mutants with altered ribonucleotide reductase: genetic model for immunodeficiency disease. *Proc. Natl. Acad. Sci. U.S.A. 76*, 1074–1078.
7. Duvic, M., Olsen, E. A., Omura, G. A., Maize, J. C., Vonderheid, E. C., Elmets, C. A., Shupack, J. L., Demierre, M. F., Kuzel, T. M., and Sanders, D. Y. (2001) A phase III, randomized, double-blind, placebo-controlled study of peldesine (BCX-34) cream as topical therapy for cutaneous T-cell lymphoma. *J. Am. Acad. Dermatol. 44*, 940–947.
8. Ealick, S. E., Babu, Y. S., Bugg, C. E., Erion, M. D., Guida, W. C., Montgomery, J. A., and Secrist, J. A., III. (1991) Application of crystallographic and modeling methods in the design of purine nucleoside phosphorylase inhibitors. *Proc. Natl. Acad. Sci. U.S.A. 88*, 11540–11544.
9. Schramm, V. L. (2002) Development of transition state analogues of purine nucleoside phosphorylase as anti-T-cell agents. *Biochim. Biophys. Acta 1587*, 107–117.
10. De Azevedo, W. F., Jr., Canduri, F., dos Santos, D. M., Silva, R. G., de Oliveira, J. S., de Carvalho, L. P., Basso, L. A., Mendes, M. A., Palma, M. S., and Santos, D. S. (2003) Crystal structure of human purine nucleoside phosphorylase at 2.3Å resolution. *Biochem. Biophys. Res. Commun. 308*, 545–552.
11. Kicska, G. A., Long, L., Horig, H., Fairchild, C., Tyler, P. C., Furneaux, R. H., Schramm, V. L., and Kaufman, H. L. (2001) Immucillin H, a powerful transition-state analog inhibitor of purine nucleoside phosphorylase, selectively inhibits human T lymphocytes. *Proc. Natl. Acad. Sci. U.S.A. 98*, 4593–4598.
12. Schramm, V. L. (2001) Transition state variation in enzymatic reactions. *Curr. Opin. Chem. Biol. 5*, 556–563.
13. Shi, W., Basso, L. A., Santos, D. S., Tyler, P. C., Furneaux, R. H., Blanchard, J. S., Almo, S. C., and Schramm, V. L. (2001) Structures of purine nucleoside phosphorylase from *Mycobacterium tuberculosis* in complexes with immucillin-H and its pieces. *Biochemistry 40*, 8204–8215.
14. Erion, M. D., Takabayashi, K., Smith, H. B., Kessi, J., Wagner, S., Honger, S., Shames, S. L., and Ealick, S. E. (1997) Purine nucleoside phosphorylase. 1. Structure-function studies. *Biochemistry 36*, 11725–11734.
15. Versees, W., Barlow, J., and Steyaert, J. (2006) Transition-state complex of the purine-specific nucleoside hydrolase of *T. vivax*: enzyme conformational changes and implications for catalysis. *J. Mol. Biol. 359*, 331–346.
16. Assenza, S. P., and Brown, P. R. (1984) Ultraviolet and fluorescence characterization of purines and pyrimidines by post-column pH manipulation. *J. Chromatogr. 289*, 355–365.
17. Bzowska, A., Koellner, G., Wielgus-Kutrowska, B., Stroh, A., Raszewski, G., Holy, A., Steiner, T., and Frank, J. (2004) Crystal structure of calf spleen purine nucleoside phosphorylase with two full trimers in the asymmetric unit: important implications for the mechanism of catalysis. *J. Mol. Biol. 342*, 1015–1032.
18. Dlugosz, M., Bzowska, A., and Antosiewicz, J. M. (2005) Stopped-flow studies of guanine binding by calf spleen purine nucleoside phosphorylase. *Biophys. Chem. 115*, 67–76.
19. Hemminki, K. (1984) Fluorescence properties off alkylated guanine derivatives. *Acta Chem. Scand. B 34*, 603–605.
20. Porter, D. J. (1992) Purine nucleoside phosphorylase. Kinetic mechanism of the enzyme from calf spleen. *J. Biol. Chem. 267*, 7342–7351.
21. Shi, W., Ting, L. M., Kicska, G. A., Lewandowicz, A., Tyler, P. C., Evans, G. B., Furneaux, R. H., Kim, K., Almo, S. C., and Schramm, V. L. (2004) *Plasmodium falciparum* purine nucleoside phosphorylase: crystal structures, immucillin inhibitors, and dual catalytic function. *J. Biol. Chem. 279*, 18103–18106.
22. Tebbe, J., Bzowska, A., Wielgus-Kutrowska, B., Schroder, W., Kazimierczuk, Z., Shugar, D., Saenger, W., and Koellner, G. (1999) Crystal structure of the purine nucleoside phosphorylase (PNP) from *Cellulomonas* sp. and its implication for the mechanism of trimeric PNPs. *J. Mol. Biol. 294*, 1239–1255.
23. Wielgus-Kutrowska, B., Antosiewicz, J. M., Dlugosz, M., Holy, A., and Bzowska, A. (2007) Towards the mechanism of trimeric purine nucleoside phosphorylases: stopped-flow studies of binding of multisubstrate analogue inhibitor 2-amino-9-[2-(phosphonomethoxy)ethyl]-6-sulfanylpurine. *Biophys. Chem. 125*, 260–268.
24. Wielgus-Kutrowska, B., and Bzowska, A. (2006) Probing the mechanism of purine nucleoside phosphorylase by steady-state kinetic studies and ligand binding characterization determined by fluorimetric titrations. *Biochim. Biophys. Acta 1764*, 887–902.
25. Wielgus-Kutrowska, B., Bzowska, A., Tebbe, J., Koellner, G., and Shugar, D. (2002) Purine nucleoside phosphorylase from *Cellulomonas* sp.: physicochemical properties and binding of substrates determined by ligand-dependent enhancement of enzyme intrinsic fluorescence, and by protective effects of ligands on thermal inactivation of the enzyme. *Biochim. Biophys. Acta 1597*, 320–334.
26. Wierzchowski, J., Stepniak, K., Bzowska, A., and Shugar, D. (2005) Spectroscopic and kinetic studies of interactions of calf spleen purine nucleoside phosphorylase with 8-azaguanine and its 9-(2-phosphonylmethoxyethyl) derivative. *Nucleosides Nucleotides Nucleic Acids 24*, 459–464.
27. Lewandowicz, A., and Schramm, V. L. (2004) Transition state analysis for human and *Plasmodium falciparum* purine nucleoside phosphorylases. *Biochemistry 43*, 1458–1468.
28. Kim, B. K., Cha, S., and Parks, R. E., Jr. (1968) Purine nucleoside phosphorylase from human erythroyctes. II. Kinetic analysis and substrate-binding studies. *J. Biol. Chem. 243*, 1771–1776.
29. Lewandowicz, A., Shi, W., Evans, G. B., Tyler, P. C., Furneaux, R. H., Basso, L. A., Santos, D. S., Almo, S. C., and Schramm, V. L. (2003) Over-the-barrier transition state analogues and crystal structure with *Mycobacterium tuberculosis* purine nucleoside phosphorylase. *Biochemistry 42*, 6057–6066.
30. Kicska, G. A., Tyler, P. C., Evans, G. B., Furneaux, R. H., Kim, K., and Schramm, V. L. (2002) Transition state analogue inhibitors of purine nucleoside phosphorylase from *Plasmodium falciparum*. *J. Biol. Chem. 277*, 3219–3225.
31. Rinaldo-Matthis, A., Wing, C., Ghanem, M., Deng, H., Wu, P., Gupta, A., Tyler, P. C., Evans, G. B., Furneaux, R. H., Almo, S. C., Wang, C. C., and Schramm, V. L. (2007) Inhibition and structure of *Trichomonas vaginalis* purine nucleoside phosphorylase with picomolar transition state analogues. *Biochemistry 46*, 659–668.
32. Miles, R. W., Tyler, P. C., Furneaux, R. H., Bagdassarian, C. K., and Schramm, V. L. (1998) One-third-the-sites transition-state inhibitors for purine nucleoside phosphorylase. *Biochemistry 37*, 8615–8621.
33. Singh, V., Evans, G. B., Lenz, D. H., Mason, J. M., Clinch, K., Mee, S., Painter, G. F., Tyler, P. C., Furneaux, R. H., Lee, J. E., Howell, P. L., and Schramm, V. L. (2005) Femtomolar transition-state analogue inhibitors of 5′-methylthioadenosine/*S*-adenosylhomocysteine nucleosidase from Escherichia coli. *J. Biol. Chem. 280*, 18265–18273.
34. Dawson, R. M. C., Elliott D., Elliott, W. H., Jones, K. M. (1986) Spectral data and pK_a values for purines, pyrimidines, nucleosides, and nucleotides, in *Data for Biochemical Research* 3rd ed., pp 103–114, Oxford University Press, New York.
35. Kline, P. C., and Schramm, V. L. (1992) Purine nucleoside phosphorylase. Inosine hydrolysis, tight binding of the hypoxanthine intermediate, and third-the-sites reactivity. *Biochemistry 31*, 5964–5973.
36. Murkin, A. S., Birck, M. R., Rinaldo-Matthis, A., Shi, W., Taylor, E. A. S. C. A., and Schramm, V. L. (2007) Neighboring group participation in the transition state of human purine nucleoside phosphorylase. *Biochemistry 46*, 5038–5049.
37. Paulus, H. (1969) A rapid and sensitive method for measuring the binding of radioactive ligands to proteins. *Anal. Biochem. 32*, 91–100.
38. Schramm, V. L. (1976) Comparison of initial velocity and binding data for allosteric adenosine monophosphate nucleosidase. *J. Biol. Chem. 251*, 3417–3424.
39. Desamero, R., Rozovsky, S., Zhadin, N., McDermott, A., and Callender, R. (2003) Active site loop motion in triosephosphate isomerase: T-jump relaxation spectroscopy of thermal activation. *Biochemistry 42*, 2941–2951.
40. Khajehpour, M., Wu, L., Liu, S., Zhadin, N., Zhang, Z. Y., and Callender, R. (2007) Loop dynamics and ligand binding kinetics in the reaction catalyzed by the *Yersinia* protein tyrosine phosphatase. *Biochemistry 46*, 4370–4378.
41. McClendon, S., Vu, D. M., Clinch, K., Callender, R., and Dyer, R. B. (2005) Structural transformations in the dynamics of Michaelis complex formation in lactate dehydrogenase. *Biophys. J. 89*, L07–09.
42. McClendon, S., Zhadin, N., and Callender, R. (2005) The approach to the Michaelis complex in lactate dehydrogenase: the substrate binding pathway. *Biophys. J. 89*, 2024–2032.
43. Dorman, D. E., and Roberts, J. D. (1970) Nuclear magnetic resonance spectroscopy: ^{13}C spectra of some common nucleotides. *Proc. Natl. Acad. Sci. U.S.A. 65*, 19–26.

44. Teijeira, M., Santana, L., and Uriarte, E. (1997) Assignment of the ^{13}C NMR spectra of some adenine, hypoxanthine and guanine carbonucleosides. *Magn. Reson. Chem. 35*, 806–807.
45. Casida, M. E. (1995) in *Recent Advances in Density Functional Methods* (Chong, D. P., Ed.), Vol. 1, World Scientific, Singapore.
46. Stratmann, R. E., Scuseria, G. E., and Frisch, M. J. (1998) An efficient implementation of time-dependent density-functional theory for the calculation of excitation energies of large molecules. *J. Chem. Phys. 109*, 8218–8224.
47. Frisch, M. J., Trucks, G. W., Schlegel, H. B., Scuseria, G. E., Robb, M. A., Cheeseman, J. R., Zakrzewski, V. G., Montgomery, J. A., Jr., Stratmann, R. E., Burant, J. C., Dapprich, S., Millam, J. M., Daniels, A. D., Kudin, K. N., Strain, M. C., Farkas, O. J., Tomasi, B. V., Cossi, M., Cammi, R., Mennucci, B., Pomelli, C., Adamo, C., Clifford, S., Ochterski, J., Petersson, G. A., Ayala, P. Y., Cui, Q., Morokuma, K., Malick, D. K., Rabuck, A. D., Raghavachari, K., Foresman, J. B., Cioslowski, J., Ortiz, J. V., Stefanov, B. B., Liu, G., Liashenko, A., Piskorz, P., Komaromi, I., Gomperts, R., Martin, R. L., Fox, D. J., Keith, T., Al-Laham, M. A., Peng, C. Y., Nanayakkara, A., Gonzalez, C., Challacombe, M., Gill, P. M. W., Johnson, B., Chen, W., Wong, M. W., Andres, J. L., Gonzalez, C., Head-Gordon, M., Replogle, E. S., and Pople, J. A. (2003) *Gaussian 03 revision B.04*, Gaussian, Pittsburgh, PA.
48. Maseras, F., and Morokuma, K. (1995) IMOMM: A new integrated ab initio + molecular mechanics optimization scheme of equilibrium structure. *J. Comput. Chem. 16*, 1170–1179.
49. Ghanem, M., Li, L., Rinaldo-Matthis, A., Wing, C., Almo, S. C., and Schramm, V. L. (2008) Altered thermodynamics from remote mutations altering human toward bovine purine nucleoside phosphorylases. *Biochemistry,* in press.
50. Li, L., Luo, M., Ghanem, M., Rinaldo-Matthis, A., Taylor, E. A., Almo, S. C., and Schramm, V. L. (2008) Residues remote from catalytic sites contribute to transition state structure in bovine purine nucleoside phosphorylase. *Biochemistry,* in press.
51. Luo, M., Li, L., Ghanem, M., and Schramm, V. L. (2008) Remote mutations alter the transition state structure of human purine nucleoside phosphorylase. *Biochemistry,* in press.
52. Lakowicz, J. (1999) *Principles of Fluorescence Spectroscopy*, 2nd ed., Kluwer Academic Publishers, Norwell, MA.
53. Vivian, J. T., and Callis, P. R. (2001) Mechanisms of tryptophan fluorescence shifts in proteins. *Biophys. J. 80*, 2093–2109.
54. O'Neil, J. D., and Hofmann, T. (1987) Tyrosine and tyrosinate fluorescence of pig intestinal Ca^{2+}-binding protein. *Biochem. J. 243*, 611–615.
55. Ealick, S. E., Rule, S. A., Carter, D. C., Greenhough, T. J., Babu, Y. S., Cook, W. J., Habash, J., Helliwell, J. R., Stoeckler, J. D., and Parks, R. E., Jr. (1990) Three-dimensional structure of human erythrocytic purine nucleoside phosphorylase at 3.2 Å resolution. *J. Biol. Chem. 265*, 1812–1820.
56. Agarwal, R. P., and Parks, R. E., Jr. (1969) Purine nucleoside phosphorylase from human erythrocytes. IV. Crystallization and some properties. *J. Biol. Chem. 244*, 644–647.
57. Oliveberg, M., Tan, Y. J., and Fersht, A. R. (1995) Negative activation enthalpies in the kinetics of protein folding. *Proc. Natl. Acad. Sci. U.S.A. 92*, 8926–8929.
58. Schramm, V. L. (2005) Enzymatic transition states: thermodynamics, dynamics and analogue design. *Arch. Biochem. Biophys. 433*, 13–26.
59. Shukla, M., Mishra, S., Kumar, A., and Mishra, P. (2000) An Ab Initio Study of Excited States of Guanine in the Gas Phase and Aqueous Media: Electronic Transitions and Mechanism of Spectral Oscillations. *J. Comput. Chem. 21*, 826–846.
60. Stoeckler, J. D., Poirot, A. F., Smith, R. M., Parks, R. E., Jr., Ealick, S. E., Takabayashi, K., and Erion, M. D. (1997) Purine nucleoside phosphorylase. 3. Reversal of purine base specificity by site-directed mutagenesis. *Biochemistry 36*, 11749–11756.
61. Jean, J. M., and Hall, K. B. (2001) 2-Aminopurine fluorescence quenching and lifetimes: Role of base stacking. *Proc. Natl. Acad. Sci. U.S.A. 98*, 37–41.
62. Ropp, P. A., and Traut, T. W. (1991) Allosteric regulation of purine nucleoside phosphorylase. *Arch. Biochem. Biophys. 288*, 614–620.
63. Wang, F., Miles, R. W., Kicska, G., Nieves, E., Schramm, V. L., and Angeletti, R. H. (2000) Immucillin-H binding to purine nucleoside phosphorylase reduces dynamic solvent exchange. *Protein Sci. 9*, 1660–1668.
64. Extinction coefficients were determined using the Protparam tool (www.expasy.org/tools/protparam/html).

BI702491D